

NATIONAL BUREAU OF STANDARDS REPORT

10 610

Progress Report

on

PETROGRAPHIC STUDY OF THE REFRACTORY
PERFORMANCE OF HIGH-FUSING DENTAL ALLOY
INVESTMENTS. PART I: HIGH-FUSING PHOSPHATE-
BONDED INVESTMENTS, SYNCHRO-X INVESTMENTS



U.S. DEPARTMENT OF COMMERCE
NATIONAL BUREAU OF STANDARDS

NATIONAL BUREAU OF STANDARDS

The National Bureau of Standards¹ was established by an act of Congress March 3, 1901. Today, in addition to serving as the Nation's central measurement laboratory, the Bureau is a principal focal point in the Federal Government for assuring maximum application of the physical and engineering sciences to the advancement of technology in industry and commerce. To this end the Bureau conducts research and provides central national services in four broad program areas. These are: (1) basic measurements and standards, (2) materials measurements and standards, (3) technological measurements and standards, and (4) transfer of technology.

The Bureau comprises the Institute for Basic Standards, the Institute for Materials Research, the Institute for Applied Technology, the Center for Radiation Research, the Center for Computer Sciences and Technology, and the Office for Information Programs.

THE INSTITUTE FOR BASIC STANDARDS provides the central basis within the United States of a complete and consistent system of physical measurement; coordinates that system with measurement systems of other nations; and furnishes essential services leading to accurate and uniform physical measurements throughout the Nation's scientific community, industry, and commerce. The Institute consists of an Office of Measurement Services and the following technical divisions:

Applied Mathematics—Electricity—Metrology—Mechanics—Heat—Atomic and Molecular Physics—Radio Physics²—Radio Engineering²—Time and Frequency²—Astrophysics²—Cryogenics.²

THE INSTITUTE FOR MATERIALS RESEARCH conducts materials research leading to improved methods of measurement standards, and data on the properties of well-characterized materials needed by industry, commerce, educational institutions, and Government; develops, produces, and distributes standard reference materials; relates the physical and chemical properties of materials to their behavior and their interaction with their environments; and provides advisory and research services to other Government agencies. The Institute consists of an Office of Standard Reference Materials and the following divisions:

Analytical Chemistry—Polymers—Metallurgy—Inorganic Materials—Physical Chemistry.

THE INSTITUTE FOR APPLIED TECHNOLOGY provides technical services to promote the use of available technology and to facilitate technological innovation in industry and Government; cooperates with public and private organizations in the development of technological standards, and test methodologies; and provides advisory and research services for Federal, state, and local government agencies. The Institute consists of the following technical divisions and offices:

Engineering Standards—Weights and Measures—Invention and Innovation—Vehicle Systems Research—Product Evaluation—Building Research—Instrument Shops—Measurement Engineering—Electronic Technology—Technical Analysis.

THE CENTER FOR RADIATION RESEARCH engages in research, measurement, and application of radiation to the solution of Bureau mission problems and the problems of other agencies and institutions. The Center consists of the following divisions:

Reactor Radiation—Linac Radiation—Nuclear Radiation—Applied Radiation.

THE CENTER FOR COMPUTER SCIENCES AND TECHNOLOGY conducts research and provides technical services designed to aid Government agencies in the selection, acquisition, and effective use of automatic data processing equipment; and serves as the principal focus for the development of Federal standards for automatic data processing equipment, techniques, and computer languages. The Center consists of the following offices and divisions:

Information Processing Standards—Computer Information—Computer Services—Systems Development—Information Processing Technology.

THE OFFICE FOR INFORMATION PROGRAMS promotes optimum dissemination and accessibility of scientific information generated within NBS and other agencies of the Federal government; promotes the development of the National Standard Reference Data System and a system of information analysis centers dealing with the broader aspects of the National Measurement System, and provides appropriate services to ensure that the NBS staff has optimum accessibility to the scientific information of the world. The Office consists of the following organizational units:

Office of Standard Reference Data—Clearinghouse for Federal Scientific and Technical Information³—Office of Technical Information and Publications—Library—Office of Public Information—Office of International Relations.

¹ Headquarters and Laboratories at Gaithersburg, Maryland, unless otherwise noted; mailing address Washington, D.C. 20234.

² Located at Boulder, Colorado 80302.

³ Located at 5285 Port Royal Road, Springfield, Virginia 22151.

NATIONAL BUREAU OF STANDARDS REPORT

NBS PROJECT

311.05-11-3110189

September 14, 1971

NBS REPORT

10 610

Progress Report

on

PETROGRAPHIC STUDY OF THE REFRACTORY PERFORMANCE OF HIGH-FUSING DENTAL ALLOY INVESTMENTS. PART I: HIGH-FUSING PHOSPHATE- BONDED INVESTMENTS, SYNCHRO-X INVESTMENTS

by

C. P. Mabie*

*Research Associate, American Dental Association
Research Unit at the National Bureau of Standards,
Washington, D. C. 20234.

This investigation is part of the dental research program conducted by the National Bureau of Standards in cooperation with the American Dental Association; the United States Army Medical Research and Development Command; the Dental Sciences Division of the School of Aerospace Medicine, USAF; the National Institute of Dental Research and the Veterans Administration.

IMPORTANT NOTICE

NATIONAL BUREAU OF STANDARDS
for use within the Government. Before
and review. For this reason, the publication
whole or in part, is not authorized
Bureau of Standards, Washington, D.C.
the Report has been specifically prepared

Approved for public release by the
Director of the National Institute of
Standards and Technology (NIST)
on October 9, 2015.

Accounting documents intended
subjected to additional evaluation
ing of this Report, either in
office of the Director, National
e Government agency for which
s for its own use.



U.S. DEPARTMENT OF COMMERCE
NATIONAL BUREAU OF STANDARDS

Petrographic Study of the Refractory
Performance of High-Fusing
Dental Alloy Investments

PART I. -- High-Fired Phosphate-Bonded Investments

Detailed X-ray and microscopic petrographic studies of high-fusing alloy investments from the viewpoint of their bonding mechanisms and their reactions with the casted alloy as they pertain to determining refractory performance have been carried out. It is thought that this knowledge will contribute to the improvement of investment materials.

Both phosphate and silica-bonded investments are used in the casting of high-fusing dental alloys. This report gives results of a study of a coarse-grained high-fired phosphate-bonded investment, Synchro-X*. This investment was selected for study primarily because it has been used extensively in high-temperature burnouts and fires where the refractory performance of phosphate-bonded investments are tested most severely.

Electron-probe and X-ray diffraction studies have been made by Allan and Asgar¹ to determine the reactions of Co-Cr-base alloy with a fine-grained phosphate-bonded investment containing a colloidal silica binder, Cermigold. Also in their study, Allan and Asgar investigated, primarily by X-ray diffraction,

* The National Bureau of Standards does not approve, commend, or endorse any proprietary product or material as a class or group, and results reported by the Bureau shall not be used in advertising or sales promotion, or to indicate either explicitly or implicitly endorsement of the product or material by the National Bureau of Standards.

investment-bonding reactions at various temperatures. However, more detailed microscopic work on the phosphate-bonded investments appeared merited. It also seemed that better X-ray identification of phases in the fired investment could be obtained by making more effort in the preparation of concentrates. These were prepared by magnetic fractionation with the Franz Isodynamic Separator, selective sizing with sieves, and heavy liquid separation using bromoform-containing solutions. Small samples of powdered concentrates were mounted as glue-cement spindles in a Debye-Scherrer camera and subjected to prolonged, 10 to 15 hours, exposures to nickel-filtered copper X-radiation.

The manufacturer states that during burnout Synchro-X investment should be fired to 920°C over a period of 1.5 to 2 hours. This investment has been recently replaced by a finer-grained phosphate investment, Synchro-X-"L", that is to be fired to 705-732°C. It is said to produce a smoother cast than the older Synchro-X and is very similar in size constitution to the Cermigold, but is not used with a colloidal silica binder.

In practice, however, dental laboratories commonly tend to fire investment-mold casings used for high-fusing alloys to the highest permissible furnace temperature. In this work the temperature used was 1000°C ± 50° — attaining this temperature with a fully loaded kiln in approximately 3.5 to 4.0 hours and with 1 to 1.5 hour soaks prior to casting. One reason why these high temperatures are used is that gas-fired kilns commonly are

heavily loaded. This heavy loading puts a severe burden on these small kilns leading to large temperature gradients both inside the kiln and inside the individual mold casings. A high-temperature setting will assure that both the outside and the inside of all molds are adequately heated in the shortest time possible and will increase the allowable time for casting. Secondly, a high-temperature set will assure that the furnace temperature will not drop below acceptable limits during rapid removal of mold casings.

These dental laboratory procedures make imperative the study of the high-temperature reactions of investments. To meet this need petrographic characterizations of the investment both before and after burnout and fire, and both at and near the investment-casting interface were made.

Characterization of the Unfired Investment: One part of Synchro-X liquid commonly is mixed with approximately four parts of investment powder by weight. This ratio varies depending upon whether the model or the outer investment is being prepared, and varies, in making the outer investment, with the diameter of the casing². Unlike the liquid used in silicate investments, Synchro-X liquid is almost all water and adds very little solid to the investment. The liquid is a dilute alkaline solution of sodium, copper, chloride, sulphate, and possibly other ions. When liquid is mixed with investment powder, the mixture readily air sets.

Petrographic and chemical analyses reveal that the investment powder was predominantly quartz and cristobalite (75 to 85%) with subordinate amounts of monoammonium phosphate (10%) and calcined magnesite, and trace amounts of heavy mineral constituents normally found in sand. Quartz and cristobalite occur in approximately equal amounts, with quartz being slightly more abundant. No tridymite was detected (Table II). Both have approximately the same size distribution, predominantly ranging in size from 100 to 10 μm , but some ^{particles} are finer. Most of the quartz grains are

tabular to prolate in shape and those of cristobalite are blocky to spherical (Figure 1). Minutely disseminated impurities, quartz blebs and gas bubbles caused the cristobalite to appear cloudy (Figure 2). A few grains are complex intergrowths of quartz and cristobalite.

The cristobalite is complexly twinned and is very finely submicrocrystalline to cryptocrystalline. Usually the cristobalite is faintly birefringent but in places appears isotropic, possibly because of overlap twinning resulting from inversion from high-temperature-stable cristobalite³. Only an average refractive index can be measured because of the fine crystallinity and minutely spaced twinning. This refractive index is 1.484 (± 0.001), typical of some synthetic low-temperature-stable cristobalite⁴.

The monoammonium phosphate constituent ($\text{NH}_4\text{H}_2\text{PO}_4$) is recognized immediately by its strong birefringence, $n_o - n_e = 0.0454$ ~~0.0495~~, refractive indices, $n_o = 1.5246$ and $n_e = 1.4792$, and uniaxial negative polarization⁵. It occurs as subspherical particles commonly ranging from 70 to 20 μm in diameter, with some finer, but infrequently up to 200 μm .

Periclase (MgO) is the predominant phase in the crushed magnesite-clinker constituent. Subordinate amounts of monticellite (CaMgSiO_4) envelop the periclase in places and help bond it into grape-like clusters (Figure 3). The high and low refractive indices of the monticellite are $n_x = 1.636 \pm 0.001$ and $n_z = 1.652 \pm 0.001$ with $n_z - n_x = 0.016 \pm 0.002$. These are essentially the same as values reported for pure iron-free

monticellite⁵. X-ray data indicate that beside periclase and monticellite very subordinate amounts of forsterite, Mg_2SiO_4 , are present (Table II). It was difficult positively to detect this phase microscopically. Individual periclase crystals commonly occur as spheres ranging from 10 to 20 μm in diameter and frequently have diameters up to 35 and down to 10 μm . The refractive index of periclase is most commonly close to 1.75. Light yellow periclase ranges slightly lower, and the deep yellow and brown periclase with higher iron contents ranges up to 1.80. The periclase contains finely disseminated sub-
($FeO_{1-n} \cdot MgO_n \cdot Fe_2O_3$)
microcrystalline magnesioferrite which is an invariable constituent of iron-rich deadburned magnesite.

Spectrographic analyses are shown in Table I. Almost all of the silicon occurs as silica in quartz and cristobalite with only a very minor amount occurring as monticellite. The magnesium is predominantly as periclase and to a minor extent as monticellite, which contains almost all of the calcium. The phosphorus occurs solely as monoammonium phosphate. Aluminum, iron and manganese probably are located mostly in the calcined magnesite. Chromite ($FeCr_2O_4$) is sometimes added in the calcination of magnesite and is the probable source of most of the chromium⁶. Boron, copper, potassium, lithium and sodium probably originate mostly in the liquid. Titanium occurs at least partly as the very rare rutile and ilmenite contaminants associated with the silica, but may be present to a large extent in the calcined

magnesite. The zinc is probably mixed into the investment as a very fine-grained calcined zinc oxide.

Characterization of the Burned Out and Fired Investment: When investment powder is mixed with liquid, the monoammonium phosphate is readily dissolved. Upon setting a gel-like appearing bond envelops many of the particles (Figure 4). Heating at 100°C causes ammonia to be evolved and ammonium and other alkali condensed phosphates to be left behind to give green strength. The very minor amounts of zinc oxide and free lime present in the calcined magnesite and possibly in the fine-grained periclase may contribute to the setting of the phosphate bond.

A tightly-bonded body results when Synchro-X investment is fired at $1000^{\circ}\text{C} \pm 50^{\circ}$ (Figures 5 to 7). The cold strength of this burned out phosphate-bonded investment is greater than that of silica-bonded investments. This greater strength is caused primarily by a higher degree of sintering due to fusion-promoted silica mobilization.

Examinations of polished and thin sections show that quartz and cristobalite grains exhibit irregular "sticky" margins (Figures 7 and 8). Quartz grains, commonly, but not everywhere, have isotropic-appearing rims with measurable refractive indices between 1.482 and 1.486 (Figure 8). Matrix between quartz and cristobalite grains has an isotropic-appearing aspect with refractive indices ranging between 1.482 and 1.490 (Figure 9). Transmitted light reveals that minute quartz crystals may

be incorporated in this matrix. Also, X-ray patterns and microscopically determined crystal shapes and indices indicate that tridymite may be present as part of the matrix (Table III, XRD-12, 24).

In some interstitial areas considerable "liquid bridging" occurs between the silica particles (Figure 7). Sinter bonds in these mobilized interstitial areas, not highly infused with magnesite clinker material, appear to consist of recrystallized silica, quartz and possibly tridymite interwoven with a vitreous constituent that appears in places to contain dendrites. This dendritic character is very noticeable in the interparticle bond constituents mobilized in the casting process.

The intimate interstitial dispersion of phosphate through the investment promotes silica fusion. This is expected since a low temperature eutectic in the binary system $P_2O_5-SiO_2$ occurs well below $1085^\circ C$ and probably below 1000° . Salt constituents present in the investment liquid (e.g., Na, Cl, Li, CuO, SO_3) are intimately co-precipitated with the phosphate and, along with fine-grained zinc oxide and possibly solubilized lime, probably help greatly to lower fusion temperatures in interstitially occurring bond micro-environments.

Microscopic examination of high-fired investment in both polished and thin sections reveals that micro-environments around particles of magnesite clinker are highly fused (Figures 10 to 17). Fusion in these regions appears much greater than elsewhere.

Monticellite from the magnesite clinker is partly to completely converted to a submicrocrystalline, moderately birefringent phase with irregular elongated crystals (Figures 15 to 17). Relict monticellite in the fired investment has refractive indices slightly higher, commonly $n_z = 1.659$ and $n_x = 1.637 \pm 0.002$, than in the original magnesite clinker. Refractive indices of the submicrocrystalline reaction product appear to be variable. Most of the low indices are between 1.622 and 1.626 and the high between 1.634 and 1.636.

X-ray patterns of concentrates particularly rich in the submicrocrystalline reaction product, XRD-10, 11, 14, 15 and 16, yield lines which are those of forsterite and others which were unidentified (Table ~~III~~^{IV}). However, the optical properties and general occurrence of most of the reacted material that has degraded in place from monticellite resemble those of $5CaO \cdot 2MgO \cdot 6SiO_2$ for which no pattern has been reported; $n_x = 1.621$, $n_y = 1.627$, $n_z = 1.635$, $2V =$ approximately $80^\circ+$.

According to Ferguson and Merwin⁸, "Mix crystals of wollastonite ($CaSiO_3$) and $5CaO \cdot 2MgO \cdot 6SiO_2$ and also $2CaO \cdot MgO \cdot SiO_2$ (akermanite) have optical properties which are intermediate so far as they have been determined". X-ray patterns indicate that additional forsterite is formed when MgO reacts with the surrounding silica (XRD-10, 14, 15 and 16 of Table IV).

Periclase (MgO) relicts in partly fused magnesite clinker have deep caries and embayments consisting of the rimming submicrocrystalline calcium-magnesium-silicate reaction product

(Figures 10, 11, 15 to 17). Magnesite-clinker concentrates from both fired and unfired investment were found to be highly magnetic indicating that some magnetite ($\text{FeO}\cdot\text{Fe}_2\text{O}_3$) and/or magnesioferrite ($\text{FeO}_{1-n}\cdot\text{MgO}_n\cdot\text{Fe}_2\text{O}_3$) is present. Reaction zones around corroded periclase, as indicated by a reddish nearly opaque appearance in the thin section of Figure 17, commonly have high concentrations of what appears to be finely-divided magnesioferrite associated with much lesser amounts of probable hematite (Fe_2O_3). Also spinel ($\text{MgO}\cdot\text{Al}_2\text{O}_3$) might be present in these zones. Close examination of the polished section photomicrographs (Figures 10 and 11) shows minute bright and apparently anisotropic corroded crystals proximal to relict periclase which may be hematite intimately mixed with magnesioferrite. Where periclase corrosion is highly progressed, caried and embayed minute magnesioferrite and hematite relicts appear to remain (Figure 12).

Liquefaction streamers from magnesite-clinker particles penetrate deeply into the surrounding investment. Submicroscopic, finely-dispersed iron oxide gives these "streamers" a yellowish appearance (Figure 14). Lath-shaped crystals (10 to 20 x 2 to 5 μm) of unknown identity are present in small amounts in these mobilized interstitial places. They have a high index (1.608 ± 0.004) and low index (1.566 ± 0.004), and are length slow with a slightly inclined extinction. The concentration of reddish ferruginous constituents at the periphery of periclase corrosion (Figure 17) and in deep liquefied embayments in periclase (Figure 14) indicates that magnesioferrite aided in fluxing the periclase. "Liquefied

streamers" radiating from magnesite clinker connect with other small "liquefied micro environments" and promote the transport of magnesium, calcium, and iron oxides (Figures 10 to 14).

That the oxide components in the calcined magnesite, particularly those of iron, promote liquefaction and sintering can be understood when it is realized that the binary system Fe_2O_3 - P_2O_5 has eutectics at 968 and 964°C⁹. The even lower eutectic which occurs in the system $\text{FeO}\cdot\text{Fe}_2\text{O}_3$ - P_2O_5 at 940°C¹⁰ makes it understandable how magnesioferrite or magnetite may promote fluxing. Reduced oxygen pressure induced by the manner in which the gas kiln is regulated, residual wax atmosphere, or the addition of graphite, as is done in one phosphate investment, may promote magnetite and wustite (FeO) formation, and therefore, possibly more extended silica and phosphate mobilization. Also, any excess lime that may be present in the calcined magnesite can initiate clinker fusion because in the system CaO - P_2O_5 a low melting eutectic (500°C) occurs with very small CaO - P_2O_5 ratios¹¹.

Thus, bonding of the Synchro-X investment occurs in the following stages:

1. Monoammonium phosphate is dissolved and on setting is coprecipitated with alkali ions including sodium, solubilized zinc oxide, any free and soluble lime that may be present in the deadburned magnesite, possibly a very minute portion of the MgO from the same source and chloride, sulfate, and other ions present in the liquid mix.

2. Ammonia is liberated under low heat of a drying oven or sunlamp, and^a condensed-phosphate bond is formed.

3. Phosphate and silica fusion induced during burnout and fire by the presence of sodium, chloride, lithium, sulfate and other ions, form⁵ sinter bonds containing quartz, tridymite and a glassy-appearing phosphate-silica constituent.

4. Periclase is fluxed by magnesioferrite in conjunction with fluxing by phosphate and silica, forming, along with MgO removed from degraded monticellite, additional forsterite, and from aluminum oxide included in the calcined magnesite, possible magnesium aluminum spinels ($Mg_{1-x}Fe_xAl_2O_4$).

5. Part of the magnesioferrite is back oxidized to what is probably hematite during the processes of step 4.

6. Further melt action occurs, leading to corrosion of periclase, silica, and the melt diffusion of ferrous and ferric oxide into the investment matrix and added promotion by dissolved iron oxide of even more extended fusion.

Characterization of Investment Surface Topography:

The surface topography of investment-free partial-denture ^{casings} cases that have not been sandblasted is a network of minute hills and valleys. Microscopic examination of the investment-casting surface of investment fragments that have been knocked free from poorly adhering alloy reveals that they also exhibit a network of hills and valleys. These key into those of the casting and are determined by the configuration of the particle

clumps along the surface of the casting-investment interface.

Effects of firing on investment-surface topography were determined by microscopic examination of the surfaces of small blocks of investment that had been fired to three different temperatures. Fourteen investment bricks (7 x 5 x 1-1/2 cm) were formed from Synchro-X standard refractory mix, poured into molds floored by one centimeter thick refractory brick and walled by two centimeter high walls of boxing wax. The liquid-powder mix was vibrated in molds to release bubbles and to obtain flat upper surfaces. After the poured investment was air dried overnight, the boxing wax was peeled off. Then the blocks were heated at 100°C for two hours in a drying oven. Upon removal from the oven, the blocks smelled heavily of liberated ammonia.

Four blocks were sawed in half and these halves were heated for one hour from room temperature to 560°C ± 10°. Four of the halves from different bricks were then transferred into a silicon carbide tube furnace set at 560°C and fired for one hour until a temperature of 940°C ± 10°C was attained. Another set of ten entire cast bricks were fired in a gas kiln in a dental laboratory according to that laboratory's procedure for Durallium alloy. This was a two-hour fire to a kiln temperature of 1050°C ± 50°.

Microscopic examination was made of the flat upper block surfaces with a 50X-dry Leitz Ultropak objective. The settings of the incident light cone and obstructing pie diaphragm were kept the same for comparative examinations.

Examinations revealed that clumping of particle aggregates increased as the severity of the firing conditions increased. This may be seen by close comparison of the microphotographs (Figure 18). Dark areas in the photographs are valleys, and the bright cloud-like areas are ridges and hills. In the 1050°C fire, knobby areas tended to form about particles of calcined magnesite. Therefore, fusion during the high fire led to an overall increase in the size of topographic irregularities.

It is to be expected that burnout-firing history will have a pronounced effect on the composition of the incipient melt developed in the investment. Incipient-melt composition and temperature will affect both the surface tension of the melt and its interparticulate penetration. Both of these factors determine particulate clumping or configuration. Therefore, it is expected that the more extensive the sinter liquefaction, induced by the combined operations of mold preheating and casting, the more severe will be investment-topographic irregularities at the casting interface and the greater the casting roughness.

Characterization of Casting Effects: The casting of high-fusing alloys into investments has two main effects, corrosive and strictly thermal. Strictly thermal effects result solely from the heat emanated from the casting and may occur partly after alloy solidification. Corrosive effects are caused by the combined effects of heat and oxidized vapors emitted by the casted alloy.

Heat dissipation by the casted melt commonly was observed in this study to heavily mobilize silica constituents 0.5 to 2 millimeters~~s~~ back of the casting-investment interface (Figures 19 to 23). This is expected since Synchro-X investment is used in the casting of Durallium alloy and this alloy does not form a very fluid bead much below 1550°C. It was experimentally determined that/^atemperature of 1550°C is sufficient to cause very extensive silica mobilization in Synchro-X. Fusion resulting from strictly thermal casting effects yields a sinter similar in constitution to those bonds formed in the high fire, i.e., bonds containing predominantly recrystallized silica and vitreous constituents — compare Figures 9 and 22.

Simple thermal fusion effects back from the casting interface do not appear extensive enough to reduce gas permeability significantly. However, different parts of the casted melt may give off differing amounts of heat. The variability in the amounts of this heat may make the investment susceptible to anisotropic deformation immediately after alloy impact. It is possible that this phenomenon could be a cause of some poor denture fits.

Corrosive Effects: Corrosive effects result from diffusion of constituents from the molten alloy at high temperatures into the investment. Commonly, these effects are evident in Synchro-X investments 10 to 60 μm back of the interface and involve extended liquefaction (Figures 21 through 23). The results

of electron-probe examinations of these interfaces agree closely with those reported for phosphate investments by Asgar¹. It was found that:

1. Chromium had diffused the most into the investment.
2. Cobalt occurred in relatively small amounts in the investment, out of proportion to its major constitutional status in the alloy, and was not nearly as abundant or deeply diffused as the chromium.
3. Manganese had diffused into the investment as deep as or deeper than the chromium, up to 80 μm , and was nearly completely vaporized from alloy immediately adjacent to the investment.
4. Iron appears to have diffused into the investment somewhat, apparently about as deep and as much as the cobalt.
5. No nickel, molybdenum, tungsten, copper, titanium or tantalum was detected in the ^{investment} interface.

Since chromium and manganese commonly occur in phosphate investments, it was thought that confirmation of the above results with an investment containing neither of these elements was desirable (Table I). Further, it was thought that prolonged contact with a molten alloy bead under a low oxygen pressure would make electronprobe interfacial-diffusion results somewhat more definitive. For this purpose, a 7 x 5 x 1-1/2 cm block of Howmet silica-bonded Rapid Set investment was prepared according to the procedure used in preparing Synchro-X blocks, but with

the mixing procedure standard for silica-bonded investment. To the set investment block a 0.25 cm thick Howmet protective coat ("Pro-G") was applied, which consisted mostly of free silica but contained appreciable amounts of zircon. After drying and setting, the coated investment block was subjected to a 1.5 hour gas kiln fire to 1177°C. A Durallium alloy shot was placed on this block and inserted into a silicon-carbide mullite-tube furnace under a very slowly flowing unpurified argon atmosphere and heated for 15 minutes at 1550°C ± 10°. The metal shot readily melted and formed an equilibrium-shaped bead 1.5 cm in diameter. The block and bead were cooled under argon flow overnight. On removal from the furnace the formerly white protective coat surface had a deep green color under the bead and at the bead margin. One to 2 mm from the bead margin was a purplish blue zone about 1 mm wide.

Direct scans with the electron probe revealed that the outer purplish blue zone had considerable amounts of chromium. However, the outer zone had essentially no cobalt but did have manganese. Green zones, as expected, were rich in chromium and contained appreciable amounts of cobalt and very small amounts of iron. As before, no tungsten, molybdenum, tantalum, or nickel were found to have entered the investment-coat substrate.

Since manganese oxides are known to produce purple-blue colors, e.g., in borax glass beads,¹² it is assumed that the blue coloration is due primarily to dissolved manganese oxide. The

approximate vapor pressures at 1550°C, in torr, are reported to be as follows:

$$\begin{aligned} \text{Mn} = 10^{1.1} > \text{Cu} = 10^{-0.9} > \text{Cr} = 10^{-1.2} > \text{Fe} = 10^{-2} > \text{Co, Ni} = 10^{-2.7} > \\ \text{Ti} = 10^{-3.9} > \text{Mo} = 10^{-9.6} > \text{W and Ta, both less than } 10^{-11.13}. \end{aligned}$$

Therefore, it is obvious that electronprobe diffusion results correspond closely to a vapor pressure sequence in which elements in the alloy with the higher vapor pressures have diffused more than those with the smaller vapor pressures. The presence of cobalt in the investment may be attributed mostly to its high concentration in the alloy, and the absence of nickel to its relatively low concentration.

To obtain large amounts of reacted material for X-ray analyses, two blocks of Synchro-X investment were reacted with Durallium-alloy pellets in a silicon carbide tube furnace. These blocks were from the previously described series fired at 1050°C. One block was fired with a pellet at 1550°C ± 20° in a slow, purified air flow for 15 minutes. Another block was fired under unpurified argon flow in the same way. At the firing temperatures, alloy was very fluid and formed well-shaped beads. All beads were cooled below 1400°C in an argon flow in less than two minutes. Cooling was allowed to proceed overnight in the furnace.

The alloy bead was observed to bloat when fired in air and after a time to become much less fluid. Alloy corrosion in air firings was, therefore, much more restricted than under argon,

where the alloy bead remained highly fluid and relatively unoxidized.

X-ray powder patterns of various reacted zones in the investment blocks were obtained. Also, a powder pattern was obtained from a reaction-product concentrate prepared by heavy liquid separation of scrapings from an investment used in casting (Table ~~III~~^{IV}).

Reaction products formed in the air fire were eskolaite (Cr_2O_3), picrochromite (MgCr_2O_4) and cristobalite. This is the same as that reported by Allan and Asgar¹. In the argon fire, picrochromite and cristobalite were formed in major amounts, but only minor amounts of eskolaite were formed. X-ray examination of the concentrate prepared from cast investment revealed that picrochromite, eskolaite and probably cristobalite were formed.

Polished sections were prepared through reacted layers at the investment-casting interface. Epi-darkfield microscopic examination of these layers revealed that zones with purple-blue internal reflections are commonly to be found slightly deeper in the investment than those with green internal reflections (Figures 24 to 26). These purplish-blue zones may owe their color to dissolved manganese oxide and the green to chromium oxide in the form of eskolaite.

Very thin sections through reaction layers from spent investment show a finely submicrocrystalline, sparkly birefringent

phase which is probably eskolaite. However, in the usual thin section the alloy-investment reaction products appear opaque (Figure 27). Mixtures of eskolaite laths and tablets commonly occur along with picrochromite and blebs of alloy in a vitreous-appearing constituent that contains many fine dendrites (Figure 28).

It appears that corrosion in the investment interface is the result of the oxidation of vapor-transported metal alloy constituents. Manganese, iron and cobalt oxide (MnO , FeO , and CoO) tend to drive reactions with silica toward low melting olivine fields. These oxides, along with the high temperature and abundant mobilizers in the investment, lead to extended silica fusion. Fused magnesium oxide combines readily with chromium to form a refractory magnesium spinel. The chromium oxide, eskolaite, is also quite refractory up to $1900^{\circ}C$. Under low oxygen pressures it appears that reactions of chromium to form picrochromite are favored. In air, the reactions of chromium oxide are shifted more toward the formation of eskolaite.

Polished sections reveal that almost all investment pores along the interface are plugged by vitreous constituents and crystalline reaction products (Figures 21 to 29). As has been suggested by Jones¹⁴, it would appear that highly viscous melt formed during casting which plugged pores to this degree might greatly cut down gas permeability during casting.

Conclusion: Phosphate investments depend for their high strength on sinter bonding mostly through fusion-induced silica recrystallization. Iron and other minor non-phosphate constituents greatly extend the degree of silica fusion. Liquefaction in the high burnout fire and during casting also induces investment interface irregularity which causes much of the cast-alloy surface roughness.

Thermal and corrosive effects from casting induce intense liquefaction in close proximity to the interface. This may, during casting, (1) cut down the ease of gas escape from the mold thus promoting casting porosity; (2) result in anisotropic mold deformation that could give a poorly fitting cast, and (3) contribute to cast-alloy roughness by induction of inter-particulate clumping in the investment.

References

1. Allan, F. C. and Asgar, Kamal. Reaction of cobalt-chromium casting alloy with investment. J. Dent. Res. 45 (No. 4) 1516-1528, 1966.
2. Durallium Products Corporation. "Manual for Durametric Technic".
3. Frondel, Clifford. "The System of Mineralogy, vol. III Silica Minerals". John Wiley and Sons, Inc., New York and London, 264-284, 1962.
4. Rogers, A. F. The Occurrence of Cristobalite. Am. J. Sci. 45 222, 1918; J. Geology 30, 211, 1922.
5. Winchell, Alexander U. and Horace. "The Microscopical Characters of Artificial Inorganic Solid Substances, Optical Properties of Artificial Minerals". Academic Press, New York, 1964.
6. Rait, J. R. "Basic Refractories, Their Chemistry and Their Performance." Interscience Publishers, Inc., New York 174-192, 1950.
7. Tien, T.-Y. and Hummel, F. A. The system $\text{SiO}_2\text{-P}_2\text{O}_5$. J. Am. Ceram. Soc. 45 (No. 9) 422-424, 1962.
8. Ferguson, J. B. and Merwin, H. E. Art. VII. The Ternary System CaO-MgO-SiO_2 . Am. J. Sci. 48 (No. 284) 81-213 1919.

9. Wentrup, Hanns. Beitrag zum System Eisen-Phosphor-Sauerstoff, Archiv für das Eisenhüttenwesen, 9. Jahrgang, Heft 1, 57-60, 1935.
10. Tromel, von Gerhard and Schwerdtfeger, Klaus. Untersuchungen im System Eisen-Phosphor-Sauerstoff. Archiv für das Eisenhüttenwesen, 34. Jahrgang, Heft 1, 55-59, 1963.
11. Kreidler, E. R. and Hummel, F. A. J. Inorganic Chem. 6 (No. 5) 891, 1967.
12. Moses, Alfred J. and Parson, C. L. "Elements of Mineralogy Crystallography and Blowpipe Analysis." D van Nostrand Co., 216-218, 1900.
13. Honig, E. W. Vapor Pressure Data for the Solid and Liquid Elements. RCA Review, Vol. 23, No. 4, 567-586, 1962.
14. Jones, Derek W. Thermal Behavior of Silica and its Application to Dental Investments, Part 1. Brit. Dent. Journal, Vol. 122, No. 3, 91-97, 1967.

Table II. X-ray Powder Pattern Data on Unfired Investment

Conc HCl Digested (XRD-26)			70/200 Very Magnetic Concentration (XRD-25)		
I	dÅ	Assign.	I	dÅ	Assign.
			vw-w	5.48	mont.
			vvw	5.16	
			w	4.82	
m	4.29	qtz.	w	4.08	mont.
vvs	4.06	crist.	w	3.86	mont. + forst. ?
			m	3.62	mont.
vvs	3.35	qtz.	w	3.34	qtz.
m-s	3.15	crist.	w	3.16	mont.
			w-m	2.905	mont.
s	2.85	crist.	vm	2.73	forst.
			m-s	2.65	mont.
			w	2.57	mont.
			w	2.52	mont. + forst.
s	2.48	crist. qtz.	f	2.46	forst. mont.
			s	2.43	peri.
			vvw	2.38	mont.
			vf	2.33	
vw	2.31	part crist.	vw	2.27	part forst.
vw	2.27	qtz.	vvf	2.20	mont.
vw	2.23	qtz.	vvf	2.16	
m	2.135	crist. qtz.	ss	2.11	peri.
vvw	2.04	qtz.	m	1.95	
vw	1.99	qtz.			
m	1.94	crist.	m	1.81	mont.
m	1.88	crist.	w	1.75	mont. + forst.
m-s	1.82	qtz	vw	1.705	mont.
vvw	1.81				

Table II. X-ray Powder Pattern Data on Unfired Investment
(cont'd)

Conc HCl Digested (XRD-26)			70/200 Very Magnetic Concentration (XRD-25)		
vvw	1.69	crist.			
vw	1.675	qtz.	vw	1.675	mont.
vvw	1.649	crist.	vf	1.643	
m	1.612	crist.	vvf	1.613	
w	1.548		m	1.579	
w	1.539	qtz.	vw	1.539	
w	1.536	crist.		1.536	
w	1.500	crist.	vvvs	1.488	peri.
vvw	1.458	qtz.	vvvf	1.446	
vvw	1.429	crist.	vvvf	1.417	
vs	1.378	qtz. qtz.	vw	1.400	
vw	1.340	crist.	f	1.350	
vvw	1.307	crist. +	vvf	1.314	
vvw	1.293	qtz.			
w	1.283	crist.			
w	1.260	qtz.			

qtz = quartz
crist. = cristobalite
mont. = monticellite
forst. = forsterite
peri. = periclase

Table III. X-ray Powder Patterns of Various Fractions of High-Fired Synchro-X Investment

XRD-12			XRD-24			XRD-11			XRD-16			XRD-14			XRD-15			XRD-10						
Minus-400 mesh Fracible constituents obtained from 100-150 mesh fraction			Minus-400 mesh Fraction obtained after plus 70 mesh disaggregation			100-150 mesh Very magnetic Fraction obtained after plus 70 mesh disaggregation			Plus-400 mesh Fraction of s disaggregated very magnetic fraction			Float from bromoform separation of minus -400 mesh disaggregated 100-150 mesh very magnetic fraction			Sink from separa- tion of XRD-14			100-150 mesh very magnetic fraction, uncrushed aspect of XRD-11						
F	d(A)	Assign.	F	d(A)	Assign.	F	d(A)	Assign.	F	d(A)	Assign.	F	d(A)	Assign.	F	d(A)	Assign.	F	d(A)	Assign.				
						w	8.11		f	8.37					vw	8.45								
vw	5.60	Sip.O. ² ?	vw	5.60		vw	5.91	Sip.O. ² ?	vw	5.14	forst.				w	5.20	forst.	m	5.11	forst.				
f	4.54	trid.	f	4.50	trid.	w	4.81	oliv.	f	4.75					f	4.90		m	4.80					
									f	4.63					m	4.37								
vw	4.29	qtz. trid.	s	4.28	qtz. trid.	w	4.3		vw	4.30	qtz. minor forst.	w	4.29	qtz. trid. ?				m	4.27	qtz. trid. -?				
ss	4.07	crist. trid.	ss	4.07	crist. trid.	w	4.2					m	4.06	crist. trid. ?	vw	4.07	crist. trid.?	ss	4.06	crist. trid. ?				
						vw	4.0	crist. trid. Sip.O. ² ?																
w-m	3.87	trid.?	w	3.87	trid.?	s	3.81	trid.? oliv.	s	3.89	forst.	m	3.90	forst.	s	3.93	forst.				s	3.86	trid.? forst.	
															m-s	3.76					m	3.70	Sip.O. ² ? part forst.	
m	3.69	Sip.O. ² ?	f	3.71	Sip.O. ² ?	m-s	3.61	oliv. -?																
w	3.66					m	3.41	oliv.	w	3.50	forst.				m	3.51	part forst.							
vw	3.46		m	3.46								w	3.48	forst.										
vw	3.36	qtz. trid.?	ss	3.34	trid.	vw	3.31	qtz. Sip.O. ² ?	f	3.35	qtz.	vs	3.35	qtz.	vw	3.38						vw	3.34	qtz.
			vw	3.23	trid.				f	3.19					w	3.20	minor crist.				w	3.21		
m	3.15	crist.	m	3.15	crist.	m-s	3.11	crist. Sip.O. ² ?				m	3.16	crist.								w	3.15	crist.
vw	3.01		vw	3.01		m-s	2.96	part oliv. ?	m	2.98	minor forst.	m	2.97	magnesi- oliv. forst. crist.	vw	2.84					w	2.95	part forst. crist.	
w	2.86	crist.	vw	2.86	crist.	s	2.77	oliv.	s	2.77	forst. -?	m-s	2.78	forst.	s	2.79	forst.				m-s	2.76	forst.	
f	2.80		f	2.80		vw	2.69	mont. or forst.	vw	2.70	mont. or forst.	vw	2.70	mont. or forst.										
w	2.73		vw	2.74	mont.-?				vw	2.57														
vw	2.66	mont.	vw	2.68	mont.-?	vw	2.52	part magnesi- oliv.	vw	2.52	forst.	s	2.51	forst.	vs	2.53	forst.					vw	2.51	forst.
			vw	2.54	trid.	vw	2.44	peri. oliv.	vw	2.45	peri. forst.	s	2.45	qtz. crist. peri. forst.	m	2.46	qtz. crist. forst.				s	2.44	qtz. + forst.	
w	2.47	qtz. crist.	m	2.46	qtz.	vw	2.42		vw	2.40	forst.				w	2.37						vw	2.34	forst.
						vw	2.35	minor oliv.	vw	2.36	part forst.	f	2.35	part forst.	w	2.37								
m	2.2857	qtz.	m-s	2.28	trid. ?	vs	2.25	qtz.	vw	2.32	part forst.	f	2.31		w	2.33								
vw	2.24	qtz.	w-m	2.24	qtz.				vw	2.28	qtz. forst.	vw	2.28	qtz. forst.	s	2.27	qtz. + forst.							
						m	2.15	oliv.	w	2.26	forst.	m	2.26	forst.										
m	2.13	qtz. minor crist.	m-s	2.13	p. qtz.				w	2.16	part forst.	w	2.16	part forst.	f	2.22								
						s	2.11	peri. qtz.	m	2.11	peri. 200	m	2.11	peri. minor crist.	m	2.17	part forst.	vw	2.12	peri. minor crist.				
vw	2.08		vw	2.07	trid.?	w	2.02	oliv.							vw	2.12	qtz.	vw	2.12	peri. minor crist.	m	2.11	peri. minor forst. minor crist.	
w	2.03		w-m	2.04					w	2.03	minor crist.				vw	2.04					w	2.02	minor crist.	
						w	1.98	qtz.	vw	2.01	forst.													
m	1.98	part qtz. crist.	m	1.93																				
						m	1.90		m	1.95		m	1.94	minor crist.	vw	1.95					w-m	1.93	crist.	
s	1.82	qtz.	m	1.88		m	1.87		f	1.86	forst.	m	1.82	part qtz.	vw	1.89	forst.	m-s	1.88	crist. minor forst.				
vw	1.78		f	1.78		vw	1.75		vw	1.79	part forst.				vw	1.80								
vw	1.75		f	1.74		vw	1.74	oliv.	f	1.75	forst.	s	1.75	forst.	vs	1.75	forst.	s	1.74	forst.				
w	1.70	part crist.	f	1.72		f	1.71		vw	1.72					f	1.73								
w	1.67	qtz.	f	1.69		f	1.69		vw	1.70	crist.				f	1.70	crist.							
w	1.663		m	1.67	qtz.	m	1.67	qtz. minor oliv.	w	1.67	minor forst.	w	1.67	part qtz.	m	1.68						w	1.67	qtz. minor forst.
			vw	1.661																				
vw	1.641	qtz.				m	1.637	minor oliv.	w	1.638	minor forst.													
m	1.612	minor crist.	vw	1.612					w	1.614	part forst.	m	1.612	minor part forst. crist.	m	1.616	part forst.	s	1.61	minor crist.				
vw	1.563					s	1.609																	
						f	1.586	minor oliv.																
s	1.543		vw	1.563		m	1.564		w	1.565		w	1.567		m	1.573								
			s	1.542	qtz.				vw	1.541	qtz. 211	m	1.543	part qtz.										
w-m	1.497	qtz. crist.							vw	1.515		vw	1.515		vw	1.516								
vw	1.482																							
vw	1.453	qtz.	vw	1.478					vw	1.490	peri. minor forst.	m	1.490	peri. minor forst. minor crist.	vw	1.488	minor forst.	s	1.48	minor forst.				
			w-m	1.454																				
vw	1.436					vw	1.436																	
w	1.429					vw	1.421																	
w	1.402																							
w-m	1.383	part qtz.																						
m	1.374	qtz.																						
w	1.352		vw	1.353																				
vw	1.340																							
w	1.302																							
w	1.290	qtz.	w	1.288	minor qtz.	w	1.287																	

oliv. = olivine
trid. = tridymite

mont. = monticellite

Table IV. X-ray Powder Patterns of Synchro-X-Alloy Reaction Products

1550°C Air Fire - 15 min. (XRD-32)			1550°C Argon Fire-15 min. (XRD-29)			1550°C Cast Sample (XRD-4)			1550°C Argon Fire-15 min. (Deep layer) (XRD-31)			1550°C Argon Fire-15 min. (Green Shallow Area) (XRD-30)		
I	d(Å)	Assign.	I	d(Å)	Assign.	I	d(Å)	Assign.	I	d(Å)	Assign.	I	d(Å)	Assign.
vw	4.81	chrom.	m	4.81	chrom.	f	5.12	forst.	m	4.62	chrom.	w-m	4.84	chrom.
			f	4.48		f	4.82	chrom.	vw	4.45		f	4.54	
			f	4.21	qtz.	vf	4.47		vw	4.25	qtz.	f	4.26	qtz.
vvs	4.07	crist.	vw	4.05	crist.	s	4.28	qtz.	vvs	4.04	crist.	vw	4.06	crist.
						w	3.98	forst.						
w	3.64	eskol.				w	3.72	very minor forst.				vw	3.63	eskol.
w	3.35	qtz.	vw	3.32	qtz.	w	3.46	min. forst.	w	3.35	qtz.	w	3.37	qtz.
w	3.13	crist.				vw	3.34	qtz.						
vw	3.04	Co ₂ P ₂ O ₇ ?	m	3.13	crist.	vf	3.24		m-s	3.13	crist.	m	3.15	crist.
						m	3.15	Crist.	f	3.04	Co ₂ P ₂ O ₇ ?			
w	2.84	crist.	vw	2.95	chrom.	w-m	2.96	minor forst.	f	2.94		vw	2.96	
			m	2.84	crist.	m	2.85	crist.	s	2.84	crist.	m-s	2.86	crist.
			f	2.77	forst.	w-m	2.77	forst.				f	2.78	forst.
			vw	2.66	eskol.	w	2.67	eskol.	vw	2.65	eskol.	w	2.66	eskol.
			f	2.58					vf	2.58				
w	2.52	chrom.	w	2.51	chrom.	vvs	2.50	crist. forst. minor eskol.	vvs	2.495	crist. chrom. minor eskol.	vs	2.50	crist. chrom. eskol.
s	2.48	eskol. crist.	s	2.48	crist. minor eskol.									
						s	2.46	qtz. minor crist.						
vw	2.41	? chrom.	f	2.42	chrom.	f	2.35	part forst.	vf	2.415	chrom.	vf	2.41	chrom.
			vf	2.34	part forst.		2.32	part forst.				vf	2.30	
							2.29	qtz.				f	2.28	qtz.
vw	2.27	? eskol.	vw	2.24	part qtz.	vw	2.25	forst.	vw	2.25	part qtz.			
							2.24	part qtz.						
w	2.18	eskol.				f	2.16	part forst.				vf	2.18	eskol.
			f	2.16	part forst.	m	2.13	crist. qtz.						
												f	2.135	qtz.
vw	2.12	crist.	w	2.11	part part crist.				w	2.12	crist.			
						m	2.10	peri. chrom.						
vw	2.09	chrom.	vw	2.08	chrom.				w	2.08	chrom.	w	2.09	chrom.
m	2.04	eskol. 202	m	2.04	minor crist.	w	2.02	minor crist.	w-m	2.025	minor crist.	w	2.03	crist.
			vf	1.98	qtz.	m	1.98	part qtz.						
w	1.93	part crist.	m	1.93	minor crist.	m	1.93	minor crist.	m	1.93	minor crist.	m	1.935	minor crist.
w	1.87	part crist.	m	1.87	part crist.	m	1.87	part crist.	m	1.87	part crist.	m	1.87	part crist.
w	1.82	eskol. minor qtz.	f	1.81	qtz.	vs	1.82	qtz.	vw	1.81	qtz. eskol.	vw	1.81	qtz. eskol.
			vf	1.76	forst.	m	1.75	crist.				vw	1.77	forst. -?
vw	1.737		f	1.73	very minor forst.				doublet vw	1.73		vw	1.74	
vf	1.695	crist.	w	1.69	part crist.	w	1.69	part crist.	w	1.69		vw	1.70	
m	1.674	eskol.				m-s	1.67	qtz. minor eskol.				w	1.67	qtz. eskol.
			f	1.665	eskol.									
						vw	1.661		vw	1.664				
						w	1.637		f	1.634				
w	1.610	chrom. crist.	m-s	1.609	chrom. minor crist.	m-s	1.609	chrom. minor crist. minor forst.?	s	1.608	chrom. minor crist.	s	1.609	part chrom. minor crist.
vw	1.574	eskol.	vw	1.571		vw	1.564		vw	1.573		vw	1.572	
vw	1.532	minor crist.	w-m	1.531		s	1.541	qtz.	w-m	1.532	minor crist.	w	1.533	minor crist.
			w-m	1.496		w	1.498	part forst.	w	1.494	minor crist.	w	1.499	
vw	1.492	part crist.				w	1.490	peri. chrom. forst.	w	1.471	chrom.	w	1.477	chrom.
vw	1.476	chrom.	w-m	1.472	part chrom.	w	1.476							
vw	1.463	eskol.				w	1.452					vf	1.453	
m	1.431	eskol. minor crist.				w-m	1.434		m	1.431	minor crist.	m	1.431	minor crist. minor eskol.
			w-m	1.428	minor crist. (?)									
			vw	1.418	part crist.	vw	1.419	part crist.				w	1.414?	
vf	1.395	chrom.-?	vw	1.397	part chrom.	w	1.396	minor forst.	vw	1.397	part chrom. minor forst.			
						m	1.382	part qtz.						
						m-s	1.372	qtz.	w	1.367		vw	1.371	part qtz.
vw	1.365	crist.	w	1.365	minor crist.									

eskol. - eskolaite
chrom. - microchromite or
magnesiocromite

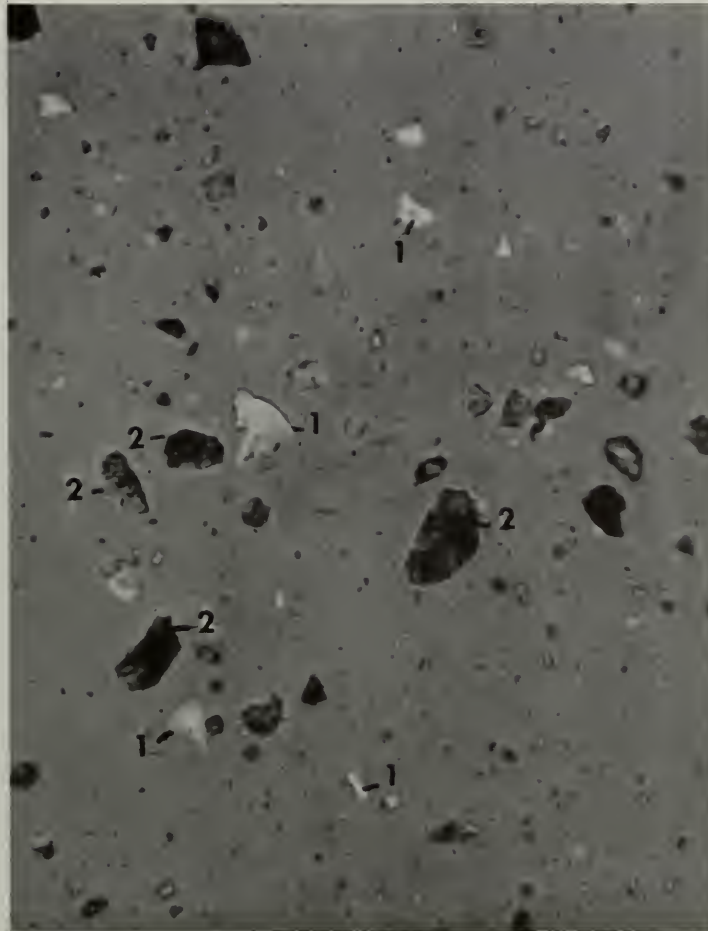


Figure 1

Synchro-X powder dispersed in Canada Balsam showing angular quartz, white birefringent grains (1), and blocky cristobalite (2); transmitted light, partly crossed nicols. X 140

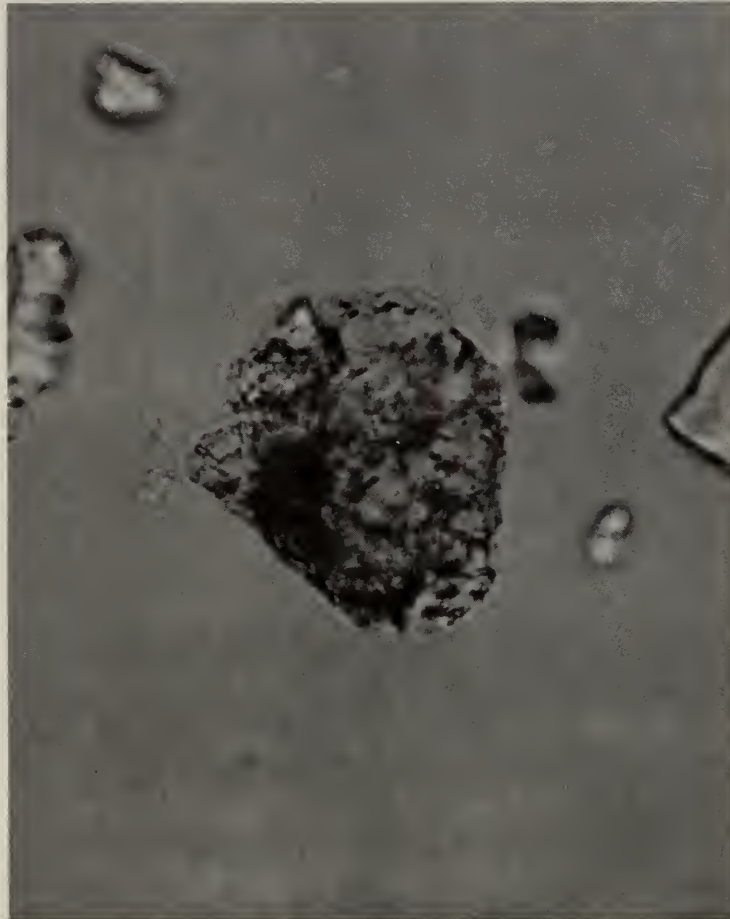


Figure 2

Synchro-X cristobalite grain showing minute disseminated quartz blebs and gas bubbles; transmitted bright-field. X 825



Figure 3

Crushed magnesite grain in Synchro-X powder showing light-colored monticellite envelopes (1) around dark periclase spheres (2); transmitted brightfield. X 825

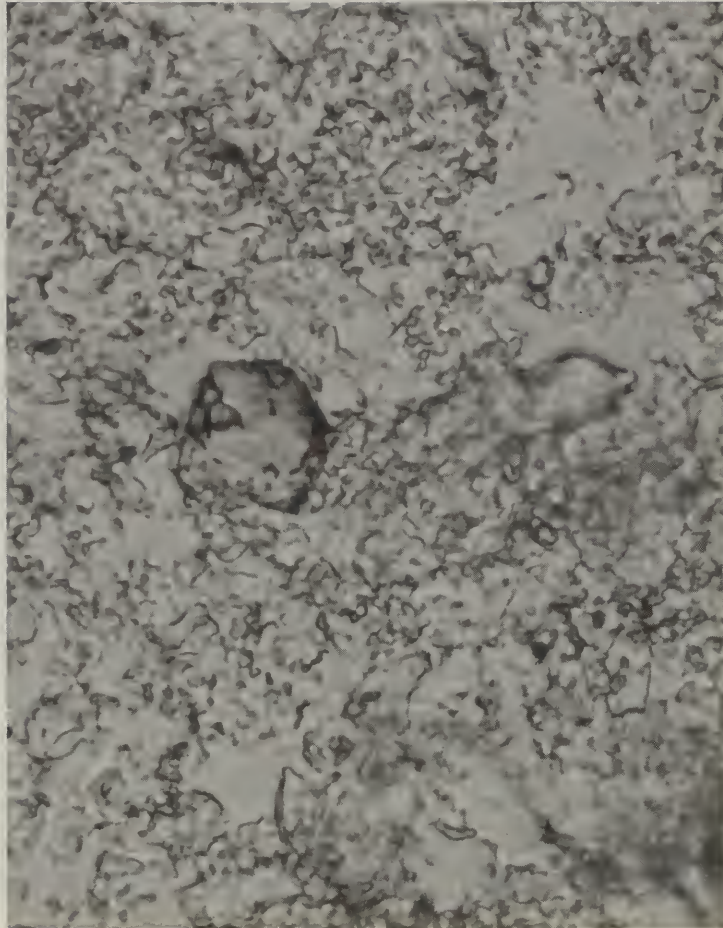


Figure 4

Ammonium phosphate gel-like bond formed on setting of the mixed Synchro-X investment under a microscope cover glass; transmitted brightfield. X 140

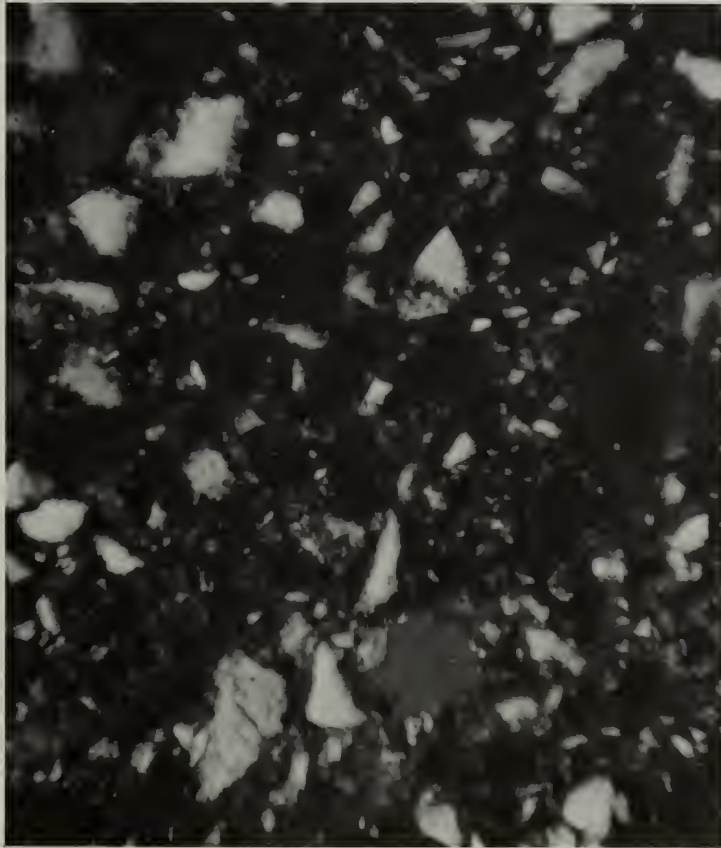


Figure 5

Thin section through fired Synchro-X investment in nearly completely polarized light. Angular to sub-rounded solidly birefringent grains are quartz. Microcrystalline to submicrocrystalline angular grains with a spotty birefringent to isotropic appearance are mostly cristobalite. Compare with same area in following photograph; transmitted polarized light. X 110

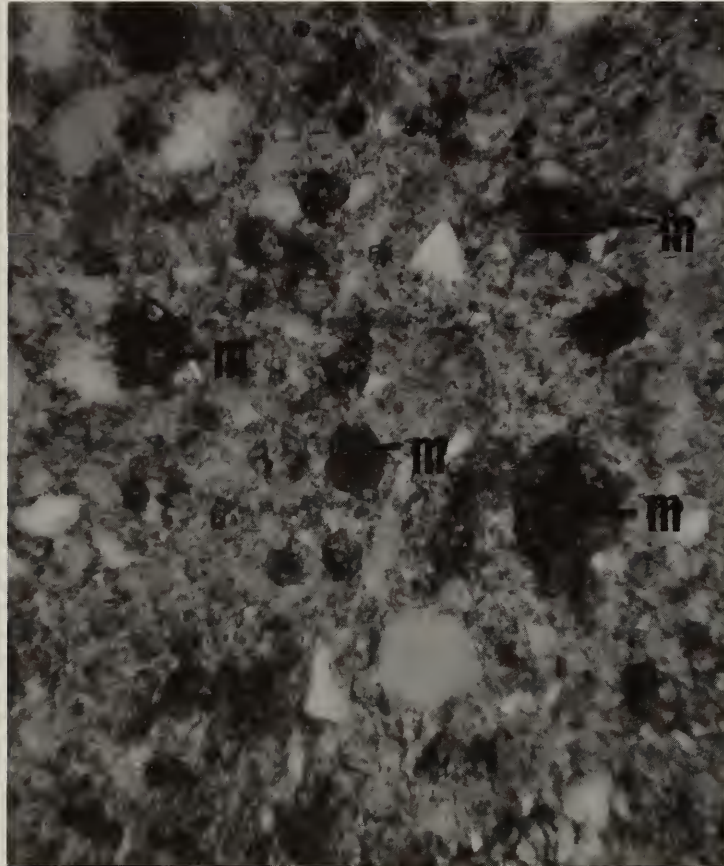


Figure 6

Thin section through fired Synchro-X investment in slightly polarized light. Angular to subrounded more birefringent grains are quartz. Light gray, poorly birefringent areas are mostly cristobalite and dark, nearly opaque zoned areas (m) are partly fused calcined magnesite. Same area as the previous photograph; transmitted slightly polarized light. X 110



Figure 7

Polished section of silica-rich region in burned-out Synchro-X investment consisting of quartz and cristobalite grains (light gray). Mounting medium occupies the darker gray areas between the light gray; epibrightfield illumination. X 700

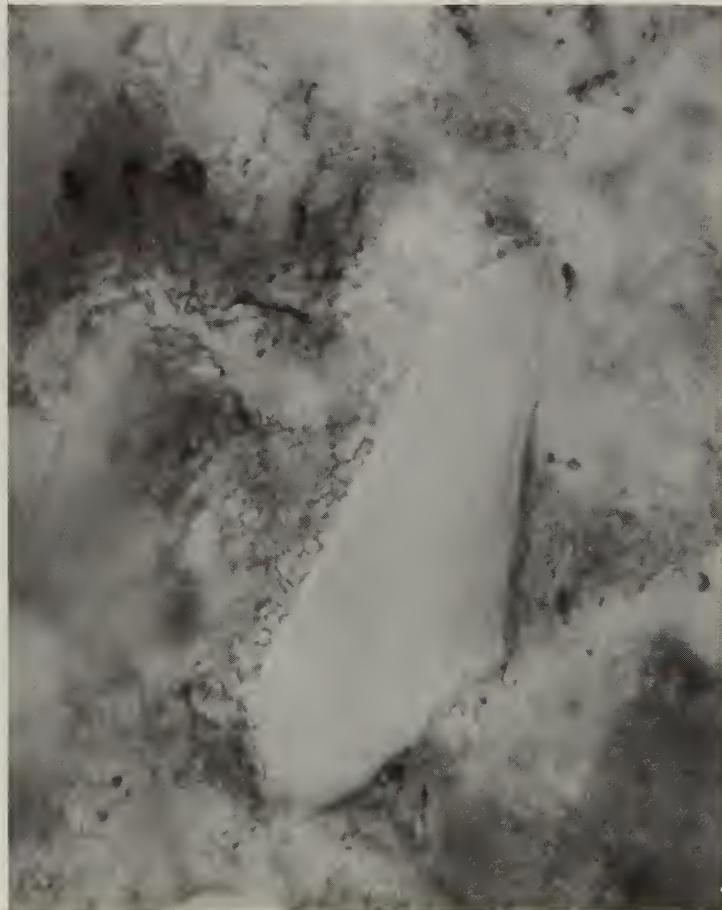


Figure 8

Thin section through quartz grain in Synchro-X investment not affected by cast-induced thermal baking showing mobilized margin probably consisting mostly of tridymite. Transmitted brightfield illumination. X 643



Figure 9

Crushed grain mount of burned-out Synchro-X with quartz fragment (q) surrounded by low index matrix material (t), probably mostly tridymite. Transmitted brightfield illumination. X 643

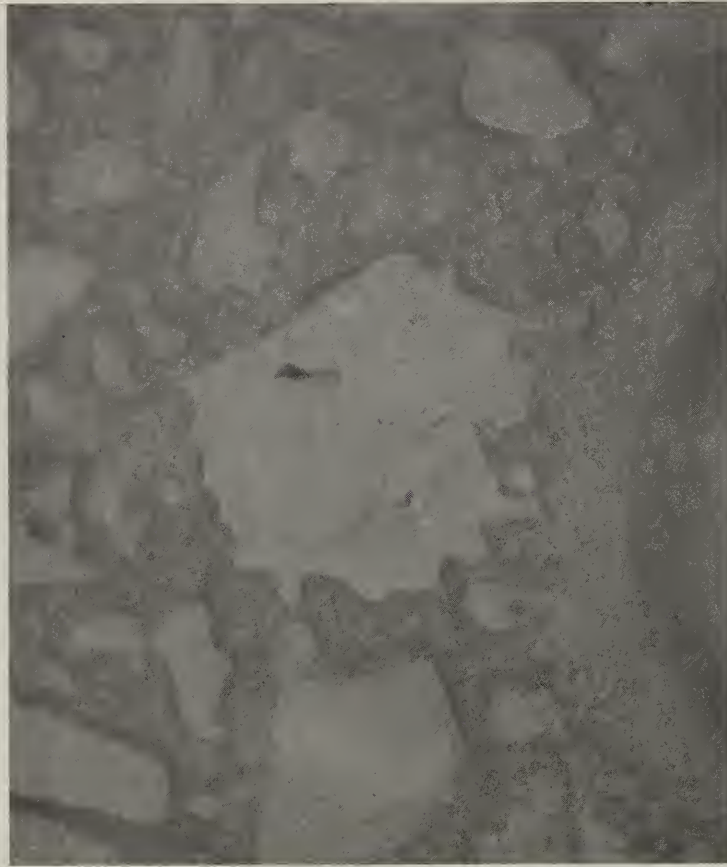


Figure 10

Polished section through partly fused magnesite inclusion (center) in burned-out and fired Synchro-X investment. Cores of rounded and embayed periclase (light gray) are rimmed by magnesium-calcium-silicate reaction product. Epi-brightfield illumination. X 700



Figure 11

Polished section through partly fused magnesite inclusion in burned-out Synchro-X investment showing "liquid bridging" (upper left) to surrounding mobilized areas. Rounded corroded periclase crystals are rimmed by fused areas consisting largely of fused magnesium-calcium-silicate reaction product. Black irregular areas in fused areas are pores. Epi-brightfield illumination. X 700



Figure 12

Polished section through fused magnesite inclusion (light medium gray) in fired Synchro-X investment showing its corrosion embayments and caries in silica (dark medium gray), mostly quartz grains. Very light gray relicts in core of fused area are probably mostly ferric oxide (hematite). Epi-brightfield illumination. X 700



Figure 13

Polished section through partly fused deadburned magnesite grain in burned-out Synchro-X investment showing a submicrocrystalline calcium-magnesium-silicate rim about periclase core (solid reddish yellow). The reddish yellow color is due to finely disseminated ferric oxide. Diffusion into the investment is delineated by light yellow stringers. Epi-brightfield illumination, oil immersion. X 700



Figure 14

Thin section of burned-out and casted Synchro-X investment probably affected by thermal baking action around magnesite inclusion with relict periclase (P, to left of center), ferric oxide blebs (deepest reddish brown) and liquefied streamers and lobes (R) penetrating into surrounding porous material. Transmitted brightfield illumination, oil immersion. X 643



Figure 15

Thin section through magnesite inclusion in burned-out Synchro-X investment showing partial reaction of monticellite envelop (bright white) around rounded periclase crystals (dark gray to black) to form magnesium-calcium-silicate (lightest gray to left). Partly polarized transmitted light, oil immersion. X 643

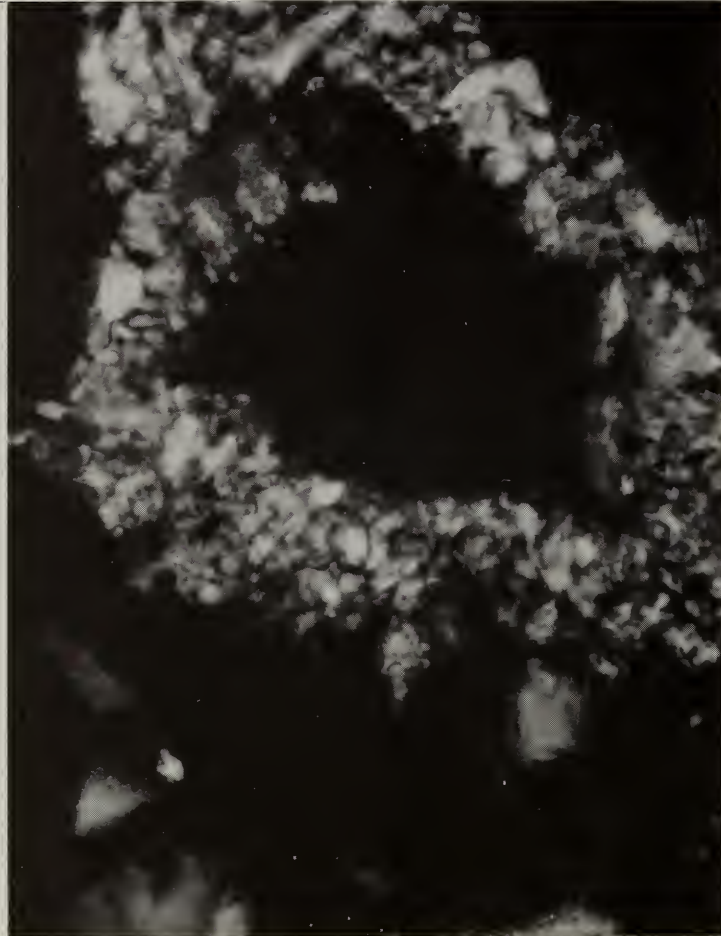


Figure 16

Thin section through partly fused magnesite inclusion in burned-out Synchro-X investment showing moderately birefringent microcrystalline magnesium-calcium-silicate reaction product (white) around periclase and ferric oxide core (black). Completely polarized transmitted light, oil immersion. X 643



Figure 17

Thin section through partly fused magnesite inclusion in burned-out Synchro-X investment showing ferric oxide rich zone (black lobaceous ring) between periclase core (dark gray) and magnesium-calcium-silicate reaction product rim (lightest gray). Same site as in previous figure. Partly polarized transmitted light, oil immersion. X 643



(a)



(b)

Figure 18

Topographic configuration of grain clusters on surface of Synchro-X investment given different heat treatments. Identical exposures, epi-darkfield illumination. X 700 (a) $1050^{\circ}\text{C} \pm 50^{\circ}$; (b) $560^{\circ}\text{C} \pm 10^{\circ}$.



Figure 19

Polished section in zone of Synchro-X investment mobilized by thermal baking resulting from casting. Fused regions of tridymite, quartz and possible vitreous material (lightest gray) carry and embay relict quartz and cristobalite. Darkest gray-to-black areas are mounting medium and unfilled voids. Center of field obstructed epi-illumination. X 700



Figure 20

Polished section exhibiting silica mobilization,
center, just below the cast-Synchro-X investment
interface at upper right. Epi-brightfield illumination.
X 700



Figure 21

Polished section showing extended interconnection of micro-environments of liquefaction below the cast of Synchro-X interface. Bright gray submicrocrystalline phases near interface are intermixed chromic oxide and magnesium-chromium spinel. Epi-brightfield illumination. X 515

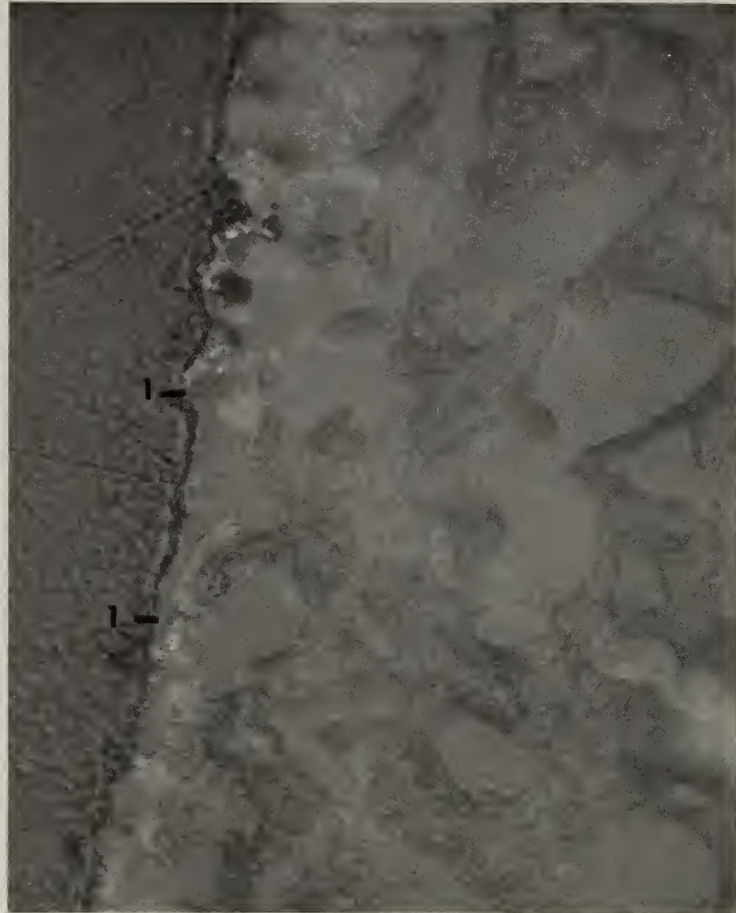


Figure 22

Polished section through liquefied Synchro-X interfacial region (1) that abutted against alloy cast exhibiting deep silica mobilization by "liquid-bridging" into investment body. White blebs in fused region are alloy, the lightest gray areas consist of chromic oxide and magnesium-chromium spinel. Solid dark-gray region along entire left margin is mounting medium. Center of field obstructed epi-illumination. X 700



Figure 23

Polished section showing limited silica mobilization beyond Synchro-X-cast interface. Epi-brightfield illumination. X 515



Figure 24

Polished section through Synchro-X interface with removed casting possibly indicating penetration of manganese (blue) deeper into the investment than chromic oxide (light green). The manganese oxide is probably largely part of a vitreous constituent. Epi-darkfield illumination. X 643



Figure 25

Polished section through alloy-casting interface of Synchro-X investment showing purplish-blue zone in the investment caused primarily by manganese oxide. Greenish crystals in very thin layer along the interface are mostly eskolaite (Cr_2O_3). Note that the casting has been removed. Epi-darkfield illumination, oil immersion. X 795



Figure 26

Polished subparallel section through alby-casting interface with intact casting (dark black at left). Greenish crystals are mostly eskolaite, minute purplish-blue regions owe their color probably to manganese oxide. Epi-darkfield illumination, oil immersion. X 795



Figure 27

Thin section through Synchro-X alloy reaction layer showing penetration of alloy reaction products, deep black opaque areas. Investment is to upper left, and mounting medium filling cast void is to lower right. Transmitted brightfield illumination. X 430



Figure 28

Polished section through magnetic concentrate of Synchro-X cast reaction layer subparallel to the interface. Note fine dendritic growths in vitreous region (v). Long bright gray crystals probably are chromic oxide; more equant bright gray grains are probably magnesium-chromium spinel. Round very bright white blebs are alloy. Cloudy milky-white areas are incompletely reacted quartz and cristobalite. Dark gray areas appear to be largely recrystallized silica. Epi-brightfield illumination. X 515



Figure 27

Thin section through Synchro-X alloy reaction layer showing penetration of alloy reaction products, deep black opaque areas. Investment is to upper left, and mounting medium filling cast void is to lower right. Transmitted brightfield illumination. X 430



Figure 28

Polished section through magnetic concentrate of Synchro-X cast reaction layer subparallel to the interface. Note fine dendritic growths in vitreous region (v). Long bright gray crystals probably are chromic oxide; more equant bright gray grains are probably magnesium-chromium spinel. Round very bright white blebs are alloy. Cloudy milky-white areas are incompletely reacted quartz and cristobalite. Dark gray areas appear to be largely recrystallized silica. Epi-brightfield illumination. X 515



Figure 29

Polished section through Synchro-X interface with casting showing greenish areas consisting mostly of submicrocrystalline chromic oxide. Void once occupied by removed casting is in upper half of photograph. Blacker regions between the greenish crystals appear highly vitreous. Epi-darkfield illumination. X 643

